Segmentation of the retinal vascular network

Vessel segmentation and detection of vessel bifurcations and crossings

Inês Rodrigues Campos , up201806778
João Santos Sousa Alves, up201806766
Maria Carolina Morgado Bastião Guedes Brás, up201704532
Matilde Carvalho Costa, up201806495

***Abstract* — This paper presents an algorithm methodology to segment retinal images and locate the feature points of the vessels. Regarding the segmentation part, it was mainly based on *Mendonça et al [1]*' s approach, considering some modifications of the parameter's values and the addition of a final morphological step. Regarding the feature points detection, although this approach was based on *Calvo, Ortega, Penedo* and *Rouco*'s work, some additional steps were conceived to improve the distinction between crossing and bifurcation points, as well as removing some wrongly identified ones. For testing the implemented algorithms, a set of training and test images/files were provided and evaluated through performance metrics. The results obtained reflected the success of the developed work.**

Keywords — component, formatting, style, styling, insert (*key words****)***

I. INTRODUCTION

The analysis of the ocular fundus is of utmost importance to diagnose or follow-up some diseases, such as diabetes and myopia. Furthermore, the quantification/location of the bifurcations and crossings on the vascular network is a common step to distinguish arteries from veins. Therefore, it is relevant to segment the vessels on the retinal images to analyse these features. Since manual segmentation is such a tiresome work, using a computer analysis, it could be executed in a much faster way.

In this work, two tasks were developed: firstly, an automatic segmentation methodology for the retinal vascular network, from a RGB eye fundus image; secondly, a detection algorithm for the vessel bifurcations/crossings' locations from a previously segmented image.

Regarding the segmentation, the algorithm implemented consists of three main phases: 1) Image preprocessing for background normalization and thin vessel enhancement; 2) Vessel centerline detection for defining a set of points in the central part of the vessel; 3) Seeded region growing to finally fill the blood vessels [1]. An ideal cross vessel profile has a similar shape as a gaussian distribution [1] with a local maximum on the center. Hence, the vessel centerlines were considered the local intensity maxima along the cross profile. To detect them, differential operators were applied in four directions. At last, the centerlines were used as seeds for an iterative region growing, whose aggregation pixels were obtained by a multiscale morphological approach with variable sized structuring elements. Regarding the feature detection, the developed algorithm involves four steps: 1) Skeletonization and pruning; 2) Intersection number calculus and feature points' identification; 3) Removal of wrongly detected/consecutive feature points; 4) Feature points' classification. The intersection number was calculated for each pixel, P, using the following equation (retrieved from [2]):

$$I(P) = {}^{1}/_{2} \left(\sum_{i=1}^{8} |N_i(P) - N_{i+1}(P)| \right) \qquad Eq.1$$

where $N_i(P)$ are the neighbours of the analyzed point, P, named clockwise consecutively. As a result, each pixel was identified as an end, internal or bifurcation/crossing point if the intersection number was, one, two or greater than two, respectively [2]. The first part of the feature points' classification was based on the number of vessel segments, $N_{vessels}$, that intersects a given circumference with radius, r, centered on each detected feature point. If $N_{vessels}$ = 3, it is identified as a bifurcation, thus, Br = 1 (otherwise, Br = 0). If $N_{vessels}$ = 4, the feature point is identified as a crossing, thus, Cr = 1 (otherwise, Cr = 0). Considering this approach for three circumferences with increasing radius R1, R2 and R3, the values of BR1, BR2, BR3, CR1, CR2 and CR3 are obtained for each pixel, P. These values were used to calculate B(P) and C(P), according to the following formulas (retrieved from [ref]):

$$C(P) = 2 \times C_{R1}(P) + C_{R2}(P) + C_{R3}(P) \qquad Eq.2$$

$$B(P) = B_{R1}(P) + B_{R2}(P) + 2 \times B_{R3}(P) \qquad Eq.3$$

The identified bifurcation points were re-analysed in the second step of the feature points' classification.

Finally, metrics such as precision, sensitivity and sensibility are calculated for the field of view of the resulted images from segmentation in relation to the ground truth. For the feature detection the recall (sensitivity) and the F-measure are calculated for each set of provided images (the training and test set), before and after the crossings and bifurcations' distinction step (F and G). These last parameters are calculated for each image and averaged in the end.

II. METHODOLOGY

A. Segmentation

In the Figure in the attchment, an overview of the implemented approach is presented.

1) Pre-Processing

a) Field of View (FOV) Reduction and Replicate Padding

Given a retinal image, the first step is decomposing the color image to three monochromatic channels (red, green, and blue). As the green channel contains the most contrasted vascular network, it is used for the intended segmentation. The given FOV mask is also used. The following images are circular and processed with filters, therefore the zeros of the background (non FOV) affect the results and non-significant content is included in the image. To decrease that influence, the best approach found was to replicate padding above the black background (which revealed less sensitivity to the background content when compared to the one that fills the zeros of the non-FOV with the mean value of the FOV – *Figure* 1 in the **Attachment**). The FOV boundary usually has high intensity values, without significant medical meaning. To ensure the replicate padding is not expanding noise and because of the reason stated, three boundary line pixels of the FOV are eliminated before the replicate padding (*Figure* 2 in the **Attachment**). After that, the replicate circular padding is done until the FOV image fulfils a circle that maximally touches on the image limits. The padded image is used in the following filter procedures, and the padded result is kept until all the filter steps end.

b) Background normalization and thin vessel enhancement

The background of the retinal images is often characterized by a gradual intensity variation occurring from the periphery of the retina toward the central macular area [1]. To evaluate only the vessels, a background estimation is done, using an average large square kernel (31x31), and the padded green image is subtracted by the background, resulting in a normalized image. Before the centerline detection, the normalized image is enhanced in the very thin vessels, usually presented with low local contrast, using four-line detection filters (*Figure* 3 in the **Attachment**), corresponding to the four orientations (0º, 45º, 90º and 135º). For each pixel, the highest filter response is kept and added to the normalized image.

2) Vessel centerline detection

The aim of this level is obtaining the vessel centerlines to seed a final region growing algorithm.

a) Candidate Selection

This step is applied to the thin vessel enhancement image.

The centerlines candidate points are obtained by using correlation with a set of difference of offset Gaussian filters (DoOG, which is a derivative filter) in four directions (0º, 45º, 90º, 135º) (figure 5 in the **Attachment**), obtaining four images. The main idea is that the center of the vessels is a local maximum and there is an intensity decrease on the direction of both vessel borders. Therefore, four patterns were next detected: "++ - -", "+ + - x" and ADV > 0, "+ x - -" and ADV < 0, "+ 0 –" (described in [1]). Next, the intensity values of the detected points are assigned with the intensity of the corresponding pixels in the thin vessel enhancement image. Finally, the obtained images are multiplied by the FOV mask because this step is the last in which a filter is applied, in the whole method.

b) Connection of candidates

In this step, the four resulted images from the previous level are processed independently to produce a set of four connected vessel segments with a common main orientation. To connect the centerline candidates, it is applied a region growing algorithm and then a correction phase. Regarding the region growing algorithm, the thresholds for the seed points and the aggregation points are calculated by intensities statistics of the candidates. Both these values are obtained by the same equations of the Mendonça et al' approach. The equation (4) for the seed selection used the intensity mean of the candidates (μ) and the standard deviation of them (σ), scaled up by a parameter α. This value was optimized (in respect to the accuracy) in our implementation, resulting in $\alpha = -0.7$, which made the selection seed criterium strict in comparison to the one used by Mendonça et al [1], proving that the training set images have lot of noise. The equation (5) reveals the aggregation criterium for the region algorithm. Regarding the labelling of the segments, it is used an eight-connectivity, so that diagonal segments don't appear labelled as different segments.

$$T_{seed} = \mu - \alpha\sigma \qquad Eq.4$$

$$T_{aggregation} = mode(I) \qquad Eq.5$$

To eliminate some noise, a correction of the centerline segments is implemented, by eliminating all the segments with a number of pixels under a stated value. This parameter was estimated to be 18 pixels. Thus, at the final of this step, there are a set of four images with a specific direction of the centerline segments.

c) Validation of Centerline Segments

In this step the candidate segments are confirmed as valid or not, based on two features: 1) the intensity of the segment (I_{seg}) and 2) the segment length. The I_{seg} is given by the geometric mean between the average and the maximum intensity value of the pixels that belong to the segment. In contrast of Mendonça et al' approach, as it is used eight-connectivity, the length of the segments does not need a different approach for diagonal or vertical and horizontal vessels. For each directional image (a set of segments), this methodology is applied and, at last, all the validate segments are compiled in a final image. This validation procedure is summarized in the flowchart (fig.6) in the attachment. For each segment of each set, the Iseg is compared with a threshold percentage of the maxima intensity of the segments from the correspondent set. The percentage threshold was optimized in our process (using the accuracy) for the training images, and it was set to 60%. The segments that do not pass in this test will be tested again, in a second validation phase, which involves the calculation of subset intensities, subset global intensities and more. This phase is extremely detailed in Mendonça et al[1] article. Afterwards, the four images are added, and the centerlines are ready to be used as seeds for the last step.

3) Multiscale vessel content segmentation

a) Multiscale morphological enhancement

In this step, it is aimed to enhance the vascular network. Because this optical structure could have different widths, a multiscale morphological approach allows to segment all the types of vessels. The morphological operator used is the top-hat transformation since the vessels represent brighter variations than the background. A classic implementation of this operator is sensitive to the noise, because all the objects, including non-pretending objects, with a radius bellow the selected structing element are enhanced. To overcome this problem, it is applied to the normalized image and it is done an adapted top-hat transform (like in Mendonça et al[1] approach), which has an additional closing operator (fig,7 in the attchment). The strategy is to apply the adapted top hat, using circular structing elements for the opening, with increasing radius [from 1 (thin vessels are enhanced) to 8 (almost all vessels are enhanced)]. For the closing operation, it is used a circular structuring element with a constant radius of 1. The eight resultant images are reduced to four, by averaging two consecutive results.

b) Multiscale reconstruction

The main idea here is to segment the resultant four images in the last step to have four different binary images with different width segmented vessels. For this purpose, it is applied a morphological reconstruction for each one of the four images. This operator uses a mask and a marker, two binary images, where the results are achieved by dilating the marker while it is contained in the mask [1]. The marker and mask images are obtained from each one of the four images, using statistical information about the histogram of them. The thresholds are set based on the percentage of pixels that are above them. As it was performed before, the best percentages were chosen by optimizing the accuracy for the training images. They are presented on table 1 in the attachment. At the end of this level, there are four segmented images, with different width vessel, which will be used in the following last procedure to fill the vessel centerlines.

4) Final Vessel Segmentation

a) Vessel Filling

After all the previous procedures, the centerlines vessels' images and the four segmented images are used to perform the final vascular network segmentation, with an iterative region growing algorithm. The centerlines are used as seeds in the first iteration and the smaller vessels' segmented image is used to fill the centerlines. In the next iteration, this result is implemented as seeds and the aggregation criterium is the reconstructed image with the following vessel width. The next two iterations are performed with the same approach.

b) Cleaning and closing operation

To the final segmentation image is applied a cleaning procedure, aiming to improve the results. All the pixels not labelled as vessels, but with at least six pixels in the neighborhood classified as vessel, are turned into vessel content; Also, if a labeled pixel vessel has less than two neighborhood pixels, it is removed. Finally, a closing operator with a disk of radius 2 as structing element is applied to unify the vessels.

B. Feature Detection

1) Skeletonization and pruning

In order to reduce the width of the vessels to one pixel, without changing their directions and the connectivity between the points, the skeleton for the image in analysis is constructed. However, the skeleton presented some unwanted small branches, that would be incorrectly considered feature points. Therefore, these components (spurs) are removed by pruning the skeleton twice.

2) Intersection number calculus

To calculate the intersection number for each pixel, firstly, the skeleton is zero-padded (1-pixel-width zero-padding). After that, the 8-neighbourhood of each pixel is analysed and, using eq.1, the intersection number is calculated for each pixel and saved in a new matrix.

3) Feature points' identification, according to the intersection number

Vessel points with an intersection number greater than two are identified as feature points for further analysis.

4) Removal of wrongly identified feature points

By plotting the obtained feature points against the original image, some are faultily marked in the background. Consequently, these points are eliminated from the group of detected feature points.

5) Removal of consecutive feature points

Since in some areas of the image several consecutive feature points are being detected, an algorithm for removing these points was developed. The 5-by-5 neighbourhood of each feature point is analysed and, if other feature points are found in that neighbourhood, those will be removed from the set of detected feature points.

6) Feature points' classification – Local analysis

The first classification step is based on the local features of the points, in other words, the number of vessel segments that create an intersection. To perform this, each detected feature point is considered as the center of three circumferences with radius R_1, R_c and R_3 ($R_1 = R_c - \rho$ and $R_3 = R_c + \rho$, where R_c was set to 4 and ρ to 2). This step consists of a voting system, according to eqs. 2 and 3, providing two values, B and C, for each feature point analysed. If C > B, the feature point is saved as a crossing. Otherwise, it is saved as a bifurcation. Note that, in order to simplify the algorithm, the circular region in analysis for each feature point is approximated by a square neighbourhood, with size equal to $2R_x - 1$.

7) Feature point classification – Topological analysis

The second classification step is based on the topological features of the pixels and aims to group together as a crossing point, two close wrongly detected bifurcation points. Once again, the neighbourhood of each pixel is studied using a circumference, with radius equal to 4 (7-by-7 square matrix). The circumference goes through the white pixels in the skeleton and, if more than one bifurcation point lies inside of it, they will no longer be considered feature points. Instead, their mean coordinates are calculated and saved as a crossing point.

III. Discussion and Results

A. Segmentation

1) Pre-Processing

a) Field of View (FOV) Reduction and Replicate Padding

In fig. 8 in the attachment, it is demonstrated one image from the testing set, where the light border line is stranded out and the padded result without the effect of the border.

b) Background normalization and thin vessel enhancement

With the background normalization, the fluctuations of the intensities were removed, and the vessels stated lighter than the background (fig.9 in the attachment). Regarding the thin vessel enhancement (fig 9 in the attachment), the 1- pixel vessels can be better distinguished from the background, after this step.

2) Vessel centerline detection

a) Candidate Selection

The images resulted from the DoOG filter shows at the cross section the pattern that it was expected. Inside the vessel, there are two hills: from the left boundary to the center a white zone (the positive responses) and from the center to the right boundary a black zone (negative responses). In fig.10 (in the attachment) are represented the results from the filters of the four directions kernel for one image of the testing set. The selection of the centerline points' candidates are shown in the fig.11 (in the attachment), accordaly the direction of the vessels.

b) Connection of candidates

After this step, all the previous selected noise, were almost eliminated and the segments are connected and labelled by eight-connectivity. It is possible to visualize the centerline segments, after the elimination of the small segments in fig.12 (in the attachment).

c) Validation of Centerline Segments

All the segments were confirmed and kept or rejected and eliminated. The final centerline segments from the previous figure were compiled in one figure. fig.13 (in the attachment)

3) Multiscale vessel content segmentation

a) Multiscale morphological enhancement

The four adapted top-hat operators allowed to enhance four ranges of vessels widths. In fig.14 (in the attachment), it is possible to verify that for the smallest structing elements, thin vessels were enhanced, for the larger structuring elements, also the larger vessels were stranded out.

b) Multiscale reconstruction

The four results of the morphological reconstruction from one image of the training set are represented in fig.15 (in the attachment). For the first reconstructed images it is possible to see some noisy points, but they are not relevant because this image fills only the centerlines.

4) Final Vessel Segmentation

a) Vessel Filling

The result from the previous image of the training set is show in fig.16 (in the attachment), as well as its vessel centerlines' image.

b) Cleaning and closing operation

In fig.17 (in the attachment) it is possible to see some corrections and improvements in cleaned image in relation to the previous result.

5) Segmentation evaluation

The mean and the standard deviation values of the accuracy, sensitivity and specificity from the FOV of the resulted images from the both sets are detailed in table 2 and 3.Also the best and worst results for both sets can be found in the attachment. It can be concluded that the testing images' results are better than the training image ones (table x in the attachment). The low standard deviation value for all the three parameters demonstrates the strength of the implemented algorithm. The mean of the sensitivity for both sets were the worst value. Indeed, looking at the best result and the worst result

from both of set images (fig x and fig y) not all the vessels could be segmented, especially the thin branches. The worst results from both sets were obtained from anormal retinal images, with big optic disc, which demonstrate another fragility of this method. For these types of images, some type of special processing could be considered in order to improve the results. Overall these results are similar to the ones obtained by Mendonça et al [1], which demonstrates the good implementation of the algorithm.

B. Feature Detection

1) Skeletonization and prunning

After the skeletonization, the skeleton spurs were successfully shortened, especially the longest ones – fig. 18 in the attachment.

2) Intersection number calculus

This step allowed the classification of the skeleton pixels as end, internal or feature points.

3) Feature points' identification, according to the intersection number

By analysing the plot of the vessels' image with the correspondent detected feature points (considering the intersection number), it was possible to conclude that the method was allowing the identification of the vessels' feature points. However, some of them were wrongly detected. The consideration of black pixels as feature points or the detection of more than one pixel for the same feature point are examples of incorrectly marked points by this method.

4) Removal of wrongly identified feature points

After the first feature points' identification, the wrongly detected pixels in the background were effectively removed – fig. 19 in the attchment.

5) Removal of consecutive feature points

Considering the 5-by-5 neighbourhood of each detected feature point, their consecutive pixels were correctly removed – fig. 20 in the attachment. Neighbourhoods with a size superior to 5 were also considered for this analysis. However, they delivered worst results, as they caused the removal of correctly detected feature points.

6) Feature points' classification – Local analysis

The explored local analysis allowed to distinguish some bifurcations from crossings. However, this method proved not to be enough to effectively perform this distinction, as it incorrectly identified some real crossings as pairs of bifurcations. Circumferences with radius greater than the utilized in this method were also analysed, resulting in a higher number of misclassified feature points.

7) Feature points' classification – Topological analysis

This analysis results in a better distinction between bifurcations and crossings than the previous one, namely when it comes to reclassifying two close bifurcations as a crossing point (fig. 19 in the attachment). Higher values for the circumference's radius were also tested. However, they resulted mainly in a decrease of the recall's mean value for a given set of images.

8) Feature detection evaluation

Regarding the training set of images, analyzing the table 4, it is possible to see that the recall values tend to be superior to the precision ones. It means that the percentage of well detected feature points relatively to all the ground truth (GT) points is higher than the percentage of well detected feature points relatively to all the points detected by the implemented methods. Therefore, it can be concluded that the explored methodology is leading to the identification of a greater total number of feature points, comparatively to the GT points. Consequently, a larger number of false positives (incorrect feature points) is being detected, which reflects the lower precision values in comparison with recall.

Although the addition of a crossings and bifurcations' distinction step provides, theoretically, a more correct feature detection, the mean value of the recall is lower for the set of images analysed with this step.

However, these results may be misleading. It should be noted that the previous metrics were calculated considering a 5-by-5 neighbourhood (a detected point is a TP, if its coordinates lay in a 5x5 square around a GT point), which means two or more distinct, but close, detected feature points may be identified in the 5-by-5 neighbourhood of the same GT point. Consequently, for the same GT point, more than one TP may be wrongly counted, increasing the value of the recall.

Taking this into consideration, when the crossings and bifurcations' distinction step is included in the image analysis, two bifurcation points, previously detected, are substituted by a crossing, that, if lays in the 5-by-5 neighbourhood of the correspondent pixel in GT, is considered as a TP. On the other hand, if this distinction step is not performed, a real crossing maybe be detected as two close bifurcations. If these bifurcations points are close enough to lay in the 5-by-5 neighbourhood of the corresponding GT crossing point, two TPs are being incorrectly considered, increasing faultily the recall value.

Regarding the testing set images, these ones exhibit better performance metrics that the previous one, as shown in table 5. This is potentially due to a better vessel segmentation of these images, which, consequently, leads to a better skeletonization and, hence, a more correct feature detection.

Regarding the crossings and bifurcations' distinction step and the performance metrics, the analysis/conclusions are identical to the explained for the previous set of images.

The best and worst results for both sets can be found in the attachment.

IV. CONCLUSION

The implemented algorithms for the segmentation and for the location of the crossings/bifurcation have extremely medical importance. The overall quantitative evaluations results are good indicative of the efficiency and accuracy of the methodologies. Some problems found and described before should be analyze to improve the results

V. REFERENCES

[1] A. M. Mendonca and A. Campilho, Segmentation of retinal blood vessels by combining the detection of centerlines and morphological reconstruction, *IEEE Transactions on Medical Imaging*, vol. 25, no. 9, pp. 1200- 1213, Sept. 2006, doi: 10.1109/TMI.2006.879955.

[2] D. Calvo, M. Ortega, M. G. Penedo and J. Rouco, "Automatic detection and characterisation of retinal vessel tree bifurcations and crossovers in eye fundus images," Computer Methods and Programs in Biomedicine, vol. 103, no. 1, pp. 28-38, Jul. 2011, doi: 10.1016/j.cmpb.2010.06.002.

VI. ATTACHMENT

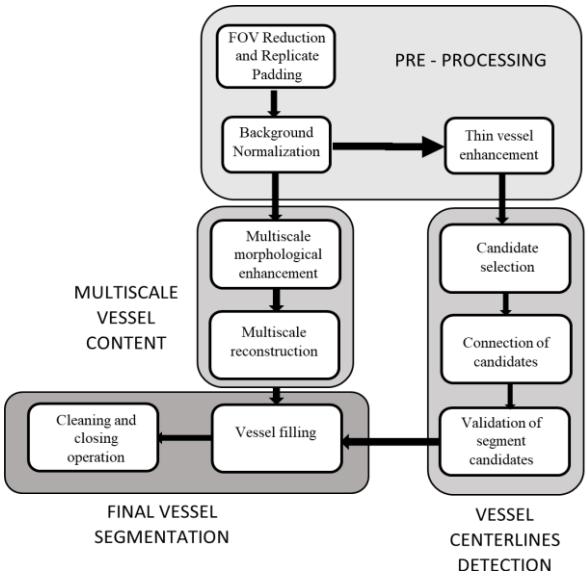

Figure 1- Flow chart of the Segmentation Process

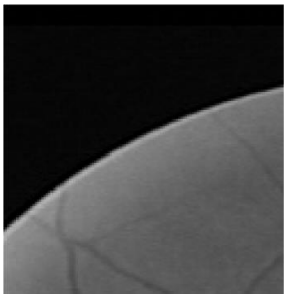

Figure 2- FOV boundary

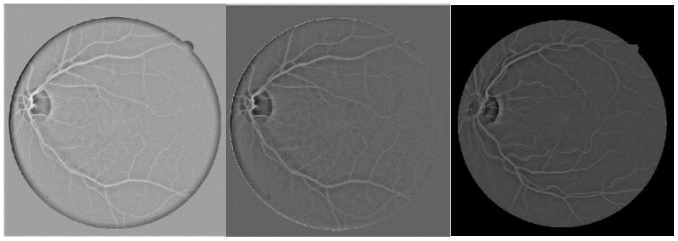

Figure 3- The effect of the non-FOV- region intensities on the normalised image. The first image is resulted from the original image with zeros in the non-FOV-region. The second is resulted from the same image with average intensity of the FOV on the non-FO- region. The third image is resulted from the same image with replicate padding on the non-FOV- region.

$$\frac{1}{6}\begin{bmatrix}-1 & -1 & -1\\ 2 & 2 & 2\\ -1 & -1 & -1\end{bmatrix};\ \frac{1}{6}\begin{bmatrix}-1 & -1 & 2\\ -1 & 2 & -1\\ 2 & -1 & -1\end{bmatrix};\ \frac{1}{6}\begin{bmatrix}-1 & 2 & -1\\ -1 & 2 & -1\\ -1 & 2 & -1\end{bmatrix};\ \frac{1}{6}\begin{bmatrix}2 & -1 & -1\\ -1 & 2 & -1\\ -1 & -1 & 2\end{bmatrix}$$

Figure 4 - Set of one-pixel width line detector filters used for thin vessel enhancement.

$$\begin{bmatrix}-1 & -2 & 0 & 2 & 1\\ -2 & -4 & 0 & 4 & 2\\ -1 & -2 & 0 & 2 & 1\end{bmatrix}$$

Figure 5 - Kernel of the DoOG filter used for enhancing variations on vertical vessels.

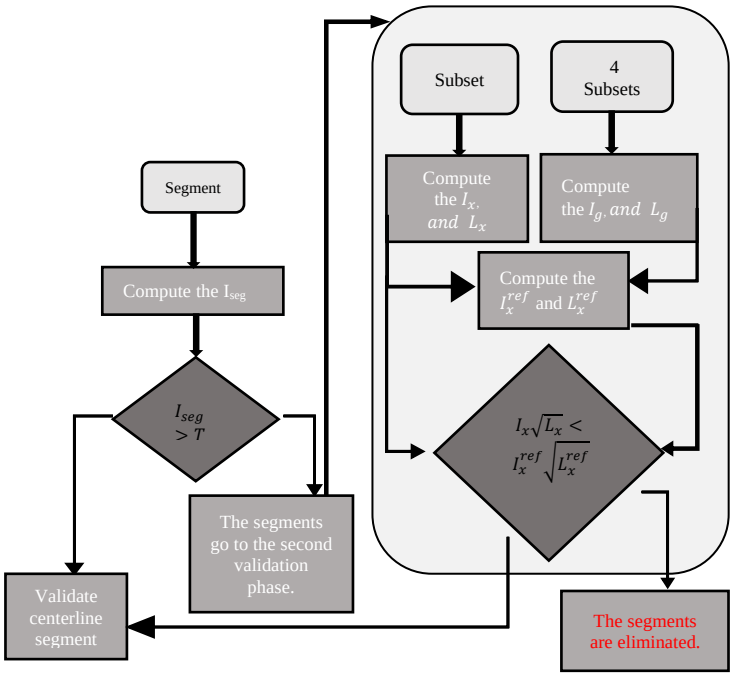

Figure 6 - Flow chart of the Validation of Centerline Segments' procedure

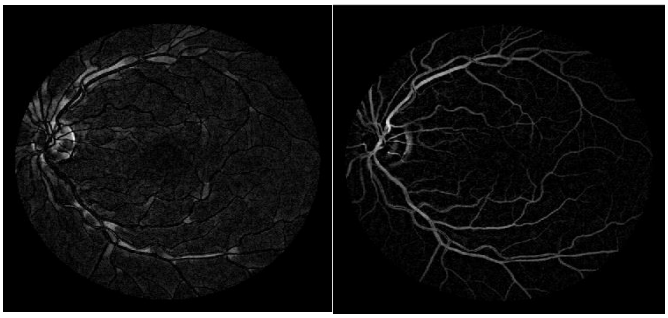

Figure *7* – Images resulted from the average of two images obtained by top-hat with two disks as structing element with radius 7 and 8. The first image is obtained by a normal top-hat operator and the seconds by the adapted top-hat operator, with a closing operator before the opening operator.

Table 1 – Seeds and grow percentages for the multiscale reconstruction

	First Image	Second Image	Third Image	Fourth Image
Seed Percentage (5)	3	2.4	1.5	0.9
Grow Percentage	0.1	0.08	0.05	0.03

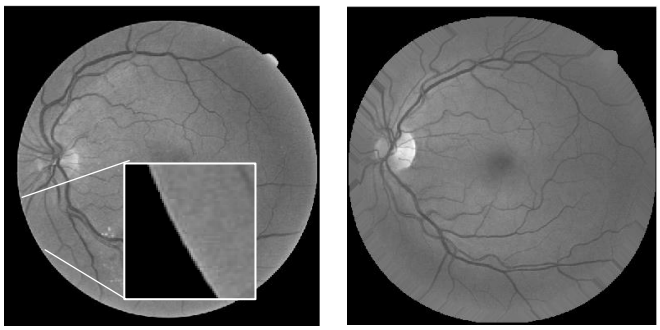

Figure *8* – Images resulted from the average of two images obtained by top-hat with two disks as structing element with radius 7 and 8. The first image is obtained by a normal top-hat operator and the seconds by the adapted top-hat operator, with a closing operator before the opening operator.

Figure *9* – Background normalization and thin vessel enhancement

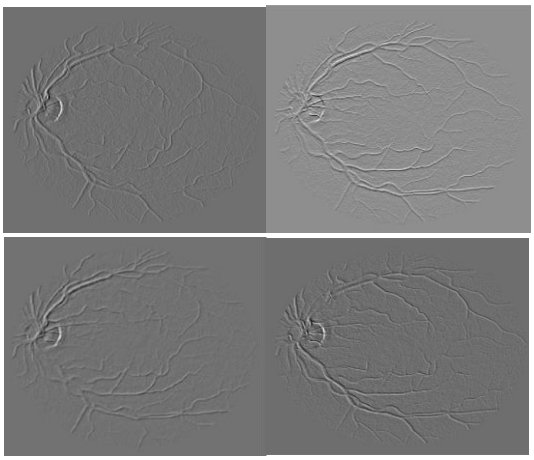

Figure *10* – Images resulted from the filter DoOG of the four directions kernel

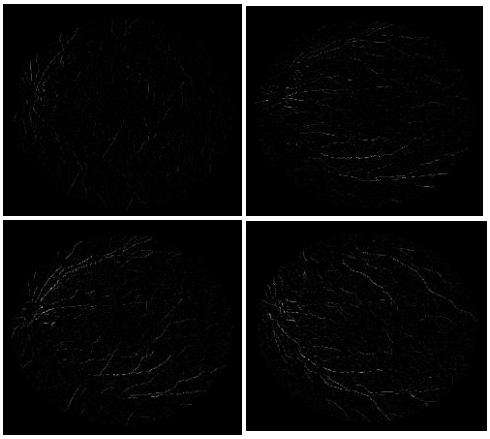

Figure *11* – Centerline Candidates for each direction

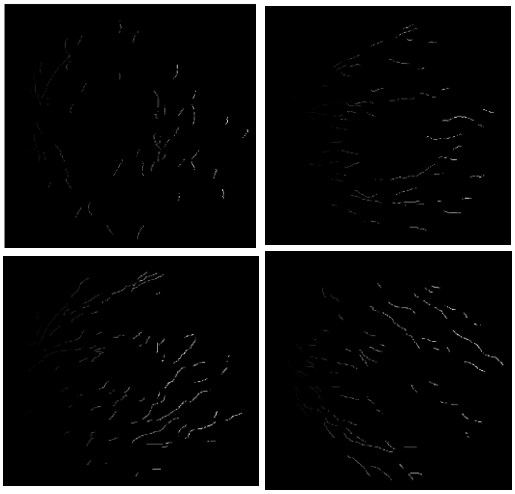

Figure *12* – Connection and cleaning of centerline points

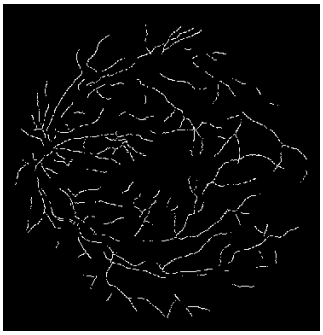

Figure *13* – Images resulted from adding the four connected and cleaned centerline points

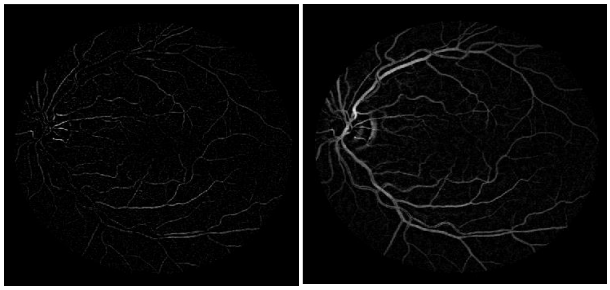

Figure ***14*** – Images resulted from the adapted tophat (left- small structing element; right larger structing element)

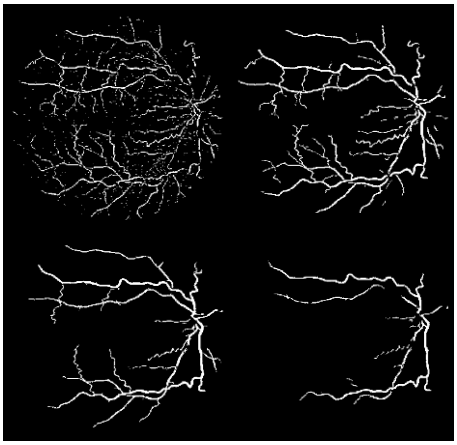

Figure ***15*** – Reconstrcuted images from the top hat results

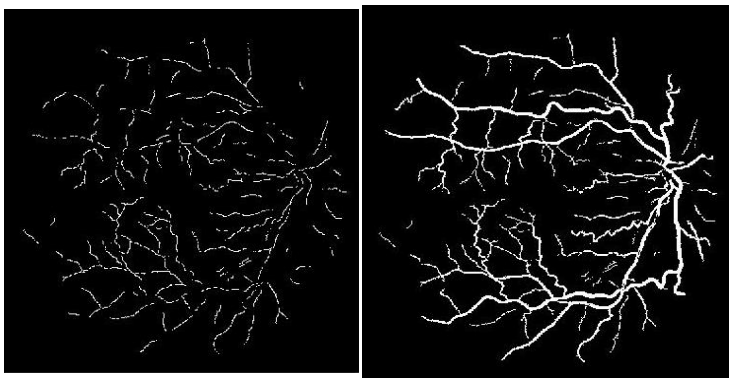

Figure *16* – Center lines and vessel filling results

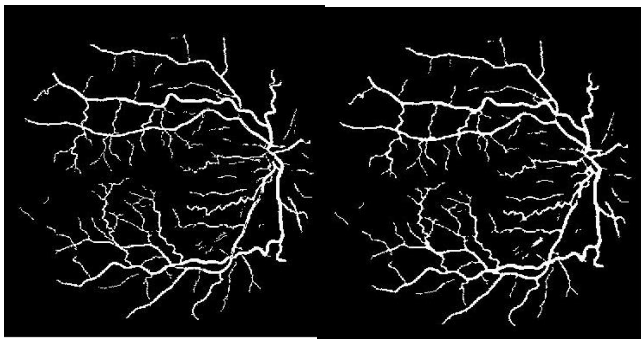

Figure 17 *– Last cleaning method (final image on right side)*

Table 2 – *Values obtained for the training set*

Training set	Mean	Std
Accuracy	0.9391	0.0085
Sensitivity	0.6992	0.0510
Specificity	0.9733	0.0113

Table 3 – *Values obtained for the test set*

Testing set	Mean	Std
Accuracy	0.9472	0.0074
Sensitivity	0.7341	0.0357
Specificity	0.9773	0.0076

Figure 18 *- Skeleton region before (left) and after (right) double pruning for spurs' removal*

Figure 19*- Image region with the identified feature points before (left) and after (right) the removal of pixels faultily considered in the image's background*

Figure 20 *- Image region with the identified feature points before (left) and after (right) the removal of the consecutive pixels of a given previously detected feature point, in a 5-by-5 neighbourhood*

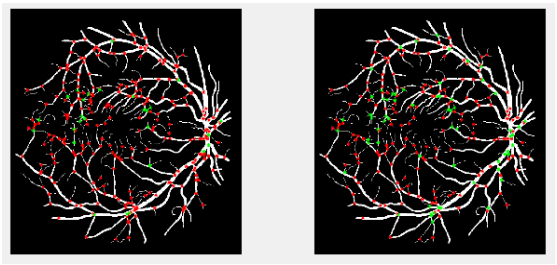

Figure 21 *- Image with the identified bifurcations (red) and crossings (green) before (left) and after (right) the topological analysis step*

Table 4 – *Mean values of the performance metrics obtained for the training set of images*

Crossings and bifurcations' distinction step	Recall	Precision	F-measure	Time
No	0.89 (0.05)	0.74 (0.06)	0.80 (0.05)	4.68 (0.96)
Yes	0.77 (0.05)	0.75 (0.06)	0.76 (0.05)	40.77 (13.93)

Table 5 – *Mean values of the performance metrics obtained for the test set of images*

Crossings and bifurcations' distinction step	Recall	Precision	F-measure	Time
No	0.88 (0.04)	0.72 (0.06)	0.79 (0.04)	5.12 (1.67)
Yes	0.78 (0.04)	0.74 (0.05)	0.76 (0.04)	49.40 (7.30)

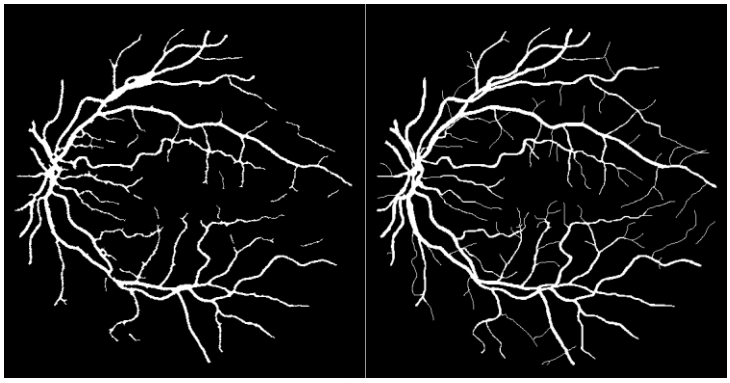

Figure 22 – Comparison between the result of the segmentation to the ground truth in the image with best accuracy of the test set

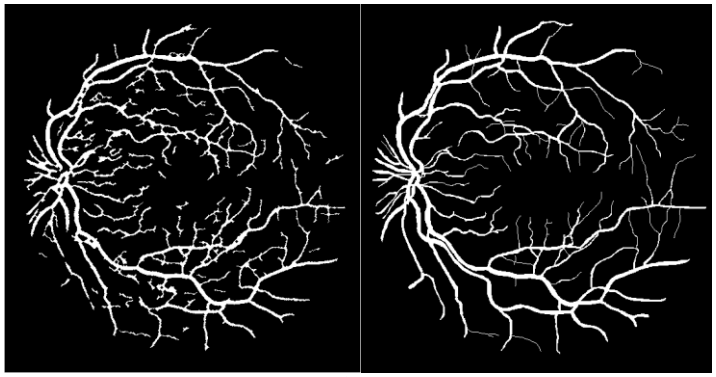

Figure 23 – Comparison between the result of the segmentation to the ground truth in the image with worst accuracy of the test set

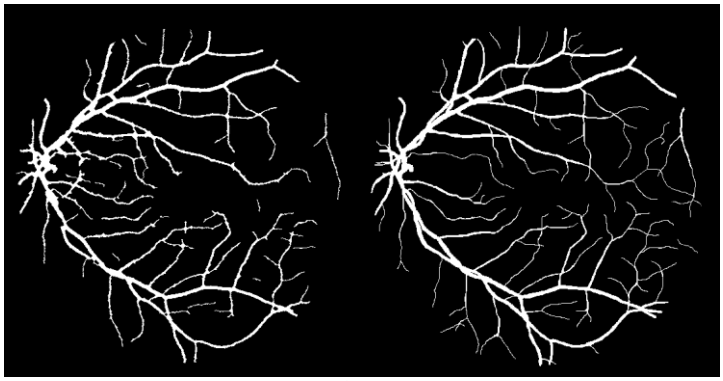

Figure 24 – Comparison between the result of the segmentation to the ground truth in the image with best accuracy of the training set

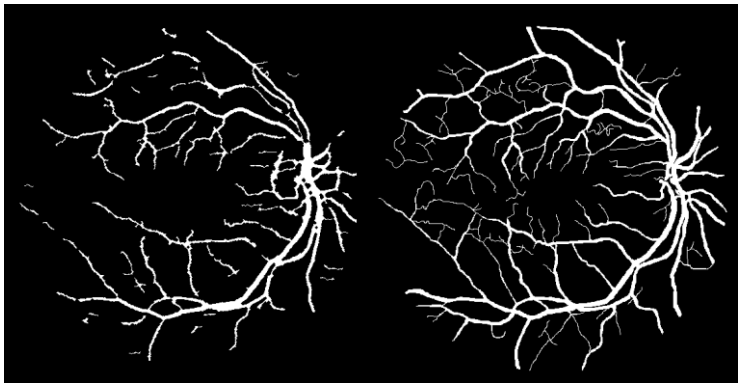

Figure 25 – Comparison between the result of the segmentation to the ground truth in the image with worst accuracy of the training set

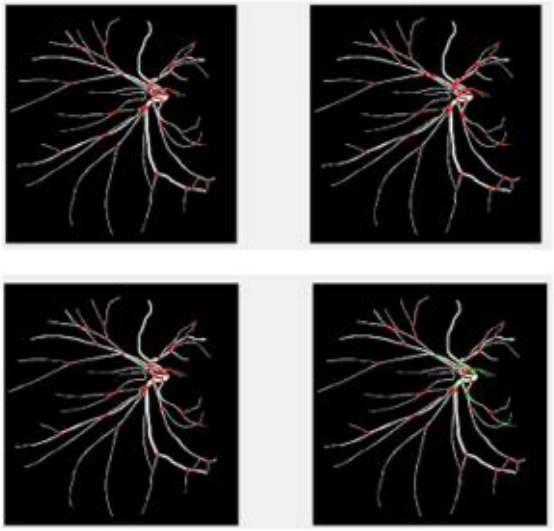

***Figure 5** - Comparison between the GT points (left) and the obtained feature points (right) with (above) and without (below) crossing/bifurcation' distinction in the image with the best recall value of the training set*

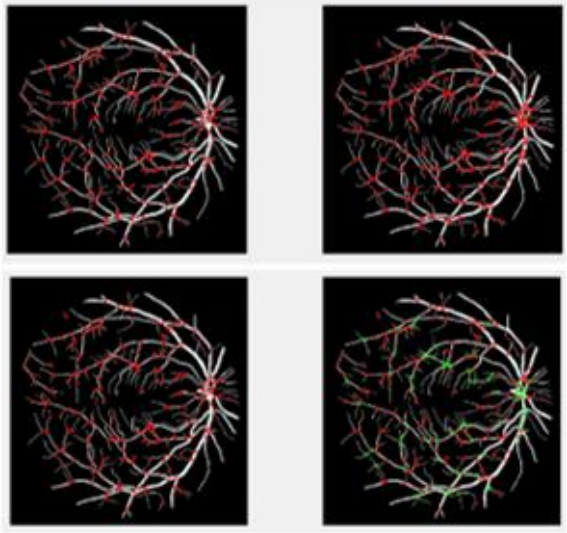

***Figure 5** - Comparison between the GT points (left) and the obtained feature points (right) with (above) and without (below) crossing/bifurcation' distinction in the image with the best recall value of the test set*

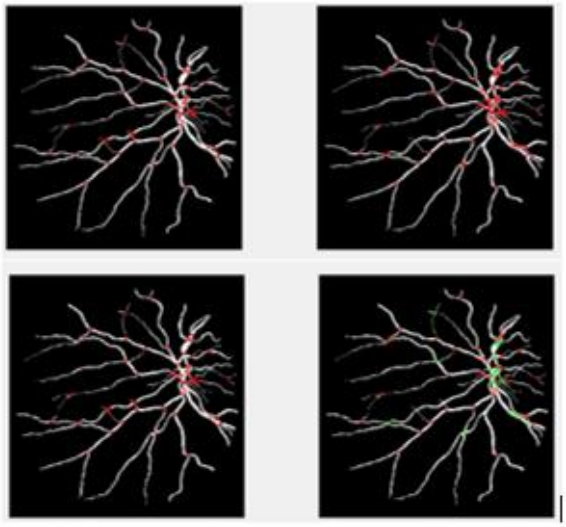

***Figure 5** - Comparison between the GT points (left) and the obtained feature points (right) with (above) and without (below) crossing/bifurcation' distinction in the image with the worst recall value of the training set*

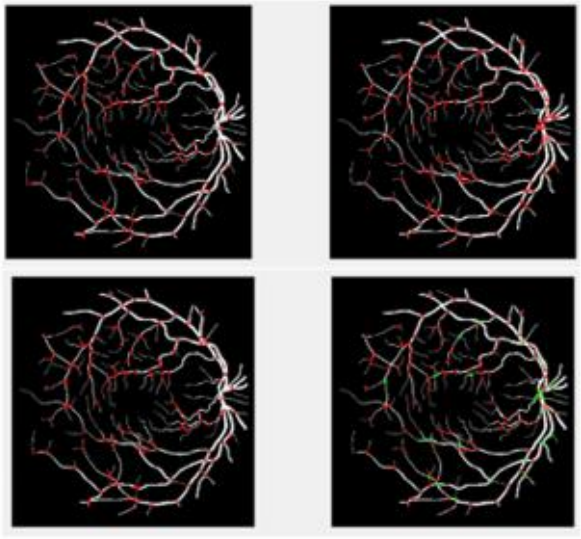

***Figure 5** - Comparison between the GT points (left) and the obtained feature points (right) with (above) and without (below) crossing/bifurcation' distinction in the image with the worst recall value of the test set*